MOLECULAR AND CELLULAR BIOLOGY, Feb. 2006, p. 1333–1346 Vol. 26, No. 4
0270-7306/06/$08.00+0 doi:10.1128/MCB.26.4.1333–1346.2006

Splicing of a Critical Exon of Human *Survival Motor Neuron* Is Regulated by a Unique Silencer Element Located in the Last Intron

Nirmal K. Singh,‡† Natalia N. Singh,† Elliot J. Androphy, and Ravindra N. Singh*

Department of Medicine, University of Massachusetts Medical School, Worcester, Massachusetts

Received 3 August 2005/Returned for modification 5 September 2005/Accepted 4 December 2005

Humans have two nearly identical copies of the *Survival Motor Neuron* (*SMN*) gene, *SMN1* and *SMN2*. In spinal muscular atrophy (SMA), *SMN2* is not able to compensate for the loss of *SMN1* due to exclusion of exon 7. Here we describe a novel inhibitory element located immediately downstream of the 5′ splice site in intron 7. We call this element intronic splicing silencer N1 (ISS-N1). Deletion of ISS-N1 promoted exon 7 inclusion in mRNAs derived from the *SMN2* minigene. Underlining the dominant role of ISS-N1 in exon 7 skipping, abrogation of a number of positive *cis* elements was tolerated when ISS-N1 was deleted. Confirming the silencer function of ISS-N1, an antisense oligonucleotide against ISS-N1 restored exon 7 inclusion in mRNAs derived from the *SMN2* minigene or from endogenous *SMN2*. Consistently, this oligonucleotide increased the levels of SMN protein in SMA patient-derived cells that carry only the *SMN2* gene. Our findings underscore for the first time the profound impact of an evolutionarily nonconserved intronic element on *SMN2* exon 7 splicing. Considering that oligonucleotides annealing to intronic sequences do not interfere with exon-junction complex formation or mRNA transport and translation, ISS-N1 provides a very specific and efficient therapeutic target for antisense oligonucleotide-mediated correction of *SMN2* splicing in SMA.

Alternative splicing increases the coding potential of the human genome by producing multiple proteins from a single gene (2). It is also associated with a growing number of human diseases (13, 15, 47). Regulation of alternative splicing is dependent upon the relative concentrations of spliceosomal and nonspliceosomal proteins, namely, serine-arginine-rich proteins (SR proteins), SR-like proteins, and heterogeneous nuclear ribonucleoproteins (hnRNPs) (16, 35, 43). Some of these proteins bind to pre-mRNA sequences called exonic splicing enhancers (ESEs), intronic splicing enhancers, exonic splicing silencers, and intronic splicing silencers (ISSs). Enhancers and silencers promote or suppress splice site (ss) selection, respectively. Over the last several years, methods have been developed to predict exonic *cis* elements (7, 12, 58). Analogous methods to predict intronic *cis* elements do not exist. Local RNA structure presents an additional level of splicing regulation. Several studies have focused on RNA structures that facilitate specific interactions during pre-mRNA splicing (3). However, the role of critical RNA structures in pre-mRNA splicing remains largely unpredictable.

Spinal muscular atrophy (SMA), the second most common autosomal recessive disorder, is caused by the absence of the *Survival of Motor Neuron 1* (*SMN1*) gene (27). *SMN1* encodes a ubiquitously expressed 38-kDa SMN protein that is necessary for snRNP assembly, an essential process for cell survival (57). A nearly identical copy of the gene, *SMN2*, fails to compensate for the loss of *SMN1* because of exon 7 skipping, producing an unstable truncated protein, SMNΔ7 (30). *SMN1* and *SMN2* differ by a critical C-to-T substitution at position 6 of exon 7 (C6U in the transcript of *SMN2*) (31, 41). C6U does not change the coding sequence but is sufficient to cause exon 7 skipping in *SMN1*. Two mutually exclusive models have been proposed to explain the inhibitory effect of C6U. According to one model, C6U abrogates an ESE associated with SF2/ASF (5), whereas another model proposes that C6U creates an exonic splicing silencer associated with hnRNP A1 (24). Based on extensive mutations, we have demonstrated that C6U creates an extended inhibitory context (Exinct) at the 3′ ss of exon 7 (Fig. 1) (50). The presence of Exinct was further supported by in vivo selection of the entire exon 7 (51).

Exon 7 is known to have a weak 3′ ss (29), probably due to its suboptimal polypyrimidine tract. An improved polypyrimidine tract promoted inclusion of exon 7 in *SMN2* (32), suggesting that the negative interactions at C6U and the positive interactions at the polypyrimidine tract are mutually exclusive. Several splicing factors have been implicated in modulation of *SMN* exon 7 splicing. Most studied among them is the SR-like protein Tra2-β1 that binds to a purine-rich ESE in the middle of exon 7 (18). Elevated expression of Tra2-β1 (18) or its associated proteins hnRNP G (19) and Srp30c (59) has been shown to promote exon 7 inclusion in *SMN2*. A recent study in which increased expression of the STAR (signal transduction and activation of RNA) family of proteins promoted exclusion of exon 7 suggests tissue-specific regulation (55). Proteins interacting with intronic sequences may also affect regulation of exon 7 splicing. Consistently, *cis* elements present in intron 6 and intron 7 have been shown to modulate exon 7 splicing (39, 40). These results highlight the complexity of pre-mRNA splic-

* Corresponding author. Mailing address: Department of Medicine (LRB 326), University of Massachusetts Medical School, 364 Plantation Street, Worcester, MA 01605. Phone: (508) 856-1333. Fax: (508) 856-6797. E-mail: Ravindra.Singh@umassmed.edu.

† N.K.S. and N.N.S. contributed equally to this work.

‡ Present address: Division of Investigative Pathology, Scott & White Clinic and Texas A&M University System Health Science Center, College of Medicine, Temple, TX 76504.

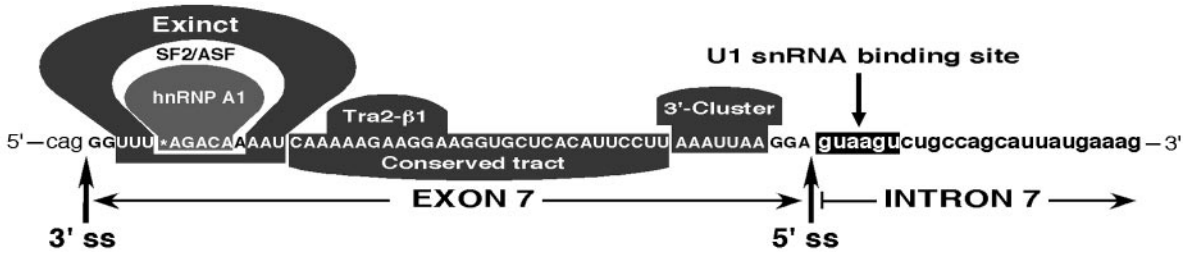

FIG. 1. Model of *cis* elements that regulate splicing of exon 7 of human *SMN*. Uppercase letters represent exon 7 sequences. Lowercase letters represent intronic sequences. The star represents position 6, where a C is replaced by a U (C6U) in *SMN2* exon 7. The U1 snRNA binding site that spans the first six nucleotides of intron 7 is shaded. Based on analysis of the entire exon 7 (51), three major *cis* elements (Exinct, Conserved tract, and 3′-Cluster) are shown. The putative binding sites of SF2/ASF (5) and hnRNP-A1 (24) fall within the inhibitory *cis* element Exinct. The binding site of Tra2-β1 (18) falls within the stimulatory *cis* element Conserved tract.

ing in which exon 7 is defined by a network of interactions involving several proteins.

Fifty-four-nucleotide-long exon 7 of human *SMN* genes contains ~65% A+U residues. Hence, exon 7 fits the typical definition of a cassette exon that generally contains a low percentage of G+C residues (9). To identify the position-specific role of residues within the entire exon, we used a systematic mutagenesis approach coupled with in vivo selection (51). This approach demonstrated for the first time the feasibility of a functional assay in which the mutability of every nucleotide within a given exon was determined (4). A highly mutable position was considered inhibitory, whereas a conserved position was considered stimulatory. Based on the mutability plot of residues within exon 7, two unique inhibitory regions, Exinct and 3′-Cluster, both rich in A+U residues, were identified (Fig. 1) (51). According to in vivo selection results, a non-wild-type guanosine residue (A54G substitution) was preferred at the last position of exon 7, indicating that the 5′ ss of exon 7 is weak. Confirming the inhibitory effect of the last adenosine residue of exon 7, A54G obviated the requirement for a number of positive elements within exon 7 (51). The mechanism by which A54G promotes exon 7 inclusion may involve enhanced recruitment of U1 snRNP due to increased base pairing between the U1 snRNA and the 5′ ss of exon 7. The strong stimulatory effect of A54G may also be associated with the rearrangement in a predicted stem-loop structure that is located at the 5′ ss (52).

Intronic sequences located immediately upstream of the 3′ ss or downstream of the 5′ ss are functionally important in splicing (38, 61). These sequences are highly diverse and could be broadly categorized into G+C-rich and A+U-rich regions that constitute distinct pentamer motifs (62). The intron 7 sequence downstream of the 5′ ss is rich in A and U residues but lacks characteristic pentamer motifs. Here we describe a novel ISS element located downstream of the 5′ ss of exon 7. We call this element ISS-N1. Our findings highlight the role of this unique intronic element in the regulation of human *SMN* exon 7 splicing. We also report that ISS-N1 provides an effective therapeutic target for the antisense oligonucleotide-mediated correction of *SMN2* splicing in SMA.

MATERIALS AND METHODS

Minigenes. Minigene splicing cassettes pSMN1ΔI6 and pSMN2ΔI6 were constructed by deleting ~6 kb within intron 6 from pSMN1 and pSMN2, respectively (50). For all of the experiments described in this report, SMN1 and SMN2 refer to pSMN1ΔI6 and pSMN2ΔI6, respectively. Mutations were generated by PCR by a strategy described earlier (50). Minigene splicing cassette *Casp3* was constructed by amplifying genomic sequences starting from exon 5 to exon 7 of the *Caspase 3* gene with high-fidelity *Pfx* polymerase (Invitrogen), genomic DNA (Clontech), and primers P53 (GTCCTCGAGTTTCTAAAGAAGATCAC AGC) and P56 (GTCGCGGCCGCACCATCTTCTCACTTGGCAT). A PCR fragment was subsequently digested with XhoI and NotI (NEB) and cloned into vector pCI (Promega). Minigene splicing cassette *Casp3*Avr was generated by inserting an AvrII restriction site (CCTAGG) into the *Casp3* minigene downstream of an alternatively spliced exon 6 by high-fidelity PCR. Minigene splicing cassette Casp3ISS-N1 was generated by inserting an ISS-N1 sequence (CCAG CATTATGAAAG) at the AvrII restriction site in Casp3Avr. For the exact locations of the AvrII and/or ISS-N1 sites, see Fig. 7C. Splicing cassettes pTBEx9-V456F (*CFTR* exon 9 splicing), pTBEx12-50A (*CFTR* exon 12 splicing), and pTBApo-ISE3m (*apoA-II* exon 3 splicing) are the same as in references 36, 45, and 46. Splicing cassettes CMV-Fas (wt) and CMV-Fas mutant (U-20C) (*Fas* exon 6 splicing) are the same as in reference 22. Splicing cassette SI9/LI10 (*Tau* exon 10 splicing) is the same as in reference 60.

Cell culture. Unless otherwise stated, all tissue culture media and supplements were purchased from Invitrogen. Human cervical carcinoma (C33a) cells, human embryonic kidney 293 (HEK-293) cells, and mouse motor neuron-like (NSC-34) cells were cultured in Dulbecco's modified Eagle's medium supplemented with 10% fetal bovine serum (FBS), 100 U/ml penicillin, and 100 μg/ml streptomycin. Human neuroblastoma (SK-N-SH) cells were maintained in a 1:1 mixture of minimum essential medium (MEM) and Ham's F12 medium supplemented with 10% FBS. Mouse neuroblastoma (Neuro-2a) cells were grown in MEM supplemented with 2 mM L-glutamine, 0.1 mM nonessential amino acids, 1.0 mM sodium pyruvate, and 10% FBS. Mouse embryonic teratocarcinoma (P19) cells were maintained in α-MEM supplemented with 10% FBS. All of the cells mentioned above were obtained from the American Type Culture Collection. NSC-34 cells were obtained from Neil Cashman (University of Toronto). Primary fibroblast cell lines from an SMA type I patient (GM03813) and a healthy control (AG06814) were obtained from Coriell Cell Repositories. These cell lines were maintained in MEM supplemented with 2 mM L-glutamine and 15% FBS.

Antisense oligonucleotides. Antisense oligoribonucleotides were synthesized by Dharmacon, Inc. The sequences of the oligonucleotides used are as follows: Anti-N1, 5′-mA*mU*mU*mC*mA*mC*mU*mU*mU*mC*mA*mU*mA*mA *mU*mG*mC*mU*mG*mG-3′; Anti-N1 + 10, 5′-mC*mA*mA*mA*mA*mG *mU*mA*mA*mG*mA*mU*mU*mC*mA*mC*mU*mU*mU*mC-3′; Anti-N1 + 20, 5′-mU*mA*mA*mA*mG*mU*mU*mU*mU*mA*mC*mA*mA *mA*mA*mG*mU*mA*mA*mG-3′; Anti-N1 + 30, 5′-mC*mC*mA*mC*mA *mA*mA*mC*mC*mA*mU*mA*mA*mA*mG*mU*mU*mU*mU*mA-3′; Scramble20, 5′-mU*mC*mC*mU*mU*mU*mA*mA*mA*mG*mU*mA*mU *mU*mG*mU*mG*mA*mC*mC; Anti-I7-25, 5′-mA*mU*mU*mC*mA*mC *mU*mU*mU*mC*mU*mA*mA*mA*mU*mU*mA*mA*mG*mG; Anti-ISS-N1/15, 5′-mC*mU*mU*mU*mC*mA*mU*mA*mA*mU*mG*mC*mU*mG *mG-3′. In these sequences, the letter m represents an *O*-methyl modification at the second position of a sugar residue and an asterisk represents a phosphorothioate modification of the backbone. Scramble20 and Anti-N1 have the same sequence composition: three guanosines, four cytosines, five adenosines, and eight uridines.

Transfections and in vivo splicing assays. All reagents were used according to the manufacturer's recommendations. Transient transfections of cells with plas-

mid DNA or antisense oligonucleotides were performed with Lipofectamine 2000 (Invitrogen). Cells were plated 24 h prior to transfection so that their density on the day of transfection was ~90%. For cotransfection experiments, cells were transfected with the indicated amounts of plasmid DNA and an oligonucleotide of interest. Oligonucleotide concentrations ranged from 25 to 500 nM. In a given experiment, the total amount of oligonucleotide was maintained constant by adding control oligonucleotide Scramble20. Unless indicated otherwise, total RNA was isolated 24 h after transfection with Trizol reagent (Invitrogen). To generate cDNA, reverse transcription was carried out with a SuperScript II reaction kit (Invitrogen). An oligo(dT) primer was used for pCI-based minigenes, while random hexamers and vector-specific 3′ primer PT2 (5′-AAGCTTGCATCGAATCAGTAG-3′) were used for pTB vector-based minigenes and *Fas* minigenes, respectively. Generally, 1.0 μg of total RNA was used per 20 μl of reaction mixture. Minigene-specific spliced products were subsequently amplified with *Taq* polymerase (Invitrogen) and the following primer combinations: P1 (5′-CGACTCACTATAGGCTAGCC-3′) and P2 (5′-GCATGCAAGCTTCCTTTTTTCTTTCCCAACAC-3′) for *SMN* minigenes (50), alfa-23 (5′-CAACTTCAAGCTCCTAAGCCACTGC-3′) and BRA2 (5′-TAGGATCCGGTCACCAGGAAGTTGGTTAAATCA-3′) for *CFTR* and *apoA-II* minigenes (36, 45, 46), FP (5′-GGTGTCCACTCCCAGTTCAA-3′) and RP (5′ CCCTGGTTTATGATGGATGTTGCCTAATGAG) for *Tau* minigenes (60), P1 and P55 (5′-GTCGCGGCCGCATCCTTTGAATTTCGCCAAG-3′) for *Casp3* minigenes, and PT1 (5′-GTCGACGACACTTGCTCAAC-3′) and PT2 for *Fas* minigenes (22). Analysis and quantifications of spliced products were performed with an FPL-5000 Image Reader and ImageGauge software (Fuji Photo Film Inc.) (50). Results were confirmed by three independent experiments.

Expression of endogenous genes. For GM03813 and AG06814 fibroblast transfection, cells were plated at a density of $\sim 0.3 \times 10^5$ per well of a 24-well plate 1 day before transfection. On the next day, cells were transfected with an oligonucleotide (from 5 to 200 nM). The total oligonucleotide amount was maintained constant by adding the Scramble20 oligonucleotide. Unless indicated otherwise, total RNA was isolated 24 h after transfection with Trizol reagent (Invitrogen). Reverse transcription was carried out with an oligo(dT) primer and SuperScript II (Invitrogen) as described above.

For PCR amplification of endogenous exons, the following primer combinations were used: N-24 (5′-CCAGATTCTCTTGATGATGCTGATGCTTTGGG-3′) and P2 (5′-GCATGCAAGCTTCCTTTTTTCTTTCCCAACAC-3′) for *SMN* exon 7, Ex4Sense (5′-CGGAATTCCAATGAAAATGAAAGCCAAGTTTCAAC-3′) and Ex6Anti (5′-ATAGTTTAGCGGCCGCCATATAATAGCCAGTATGATAG-3′) for *SMN* exon 5, Ex1Sense (5′-CGGAATTCCATGGCGATGAGCAGCGGCGGCAG-3′) and Ex4Anti (5′-ATAGTTTAGCGGCCGCCTTTCCTGGTCCCAGTCTTGG-3′-) for *SMN* exon 3, P53 and P56 for *Caspase 3* exon 6, 5′-Sur (GCATGGGTGCCCCGACGTTG) and 3′-Sur (GCTCCGGCCAGAGGCCTCAA) for *Survivin* exons 2B/3 (34), A1 (CATGAGCGACAGCGG-CGAGCAGAA) and A3 (TTAATAGCGACGAGGTGAGTA) for Tra2 exons 2a/2b (8), 5′Bcl-X (CATGGCAGCAGTAAAGCAAG) and 3′Bcl-X (GCATTGTTCCCATAGAGTTCC) for Bcl-x exon 2 (37), and ex28F (GGAGTACACCAAGTATCATGAG) and ex31R (CATTATGCTTGCAAAAACGAAC) for NF1 exons 29/30 (48). Results were confirmed by three independent experiments.

Antibodies and Western blot analysis. Transfections with antisense oligonucleotides were done as described above. For each sample, the same number of cells ($\sim 9 \times 10^5$) was harvested 72 h after transfection and lysates were prepared as described in reference 11. One-third of each lysate was used for one blot. Lysates were electrophoresed on a 10% (wt/vol) sodium dodecyl sulfate-polyacrylamide gel electrophoresis gel, and the proteins were transferred onto polyvinylidene fluoride membrane (Pall Life Sciences). The protein transfer and equal loading were verified by SYPRO Ruby protein blot staining (Bio-Rad Laboratories). The membranes were blocked with 5% nonfat dried milk in TBST (20 mM Tris, 150 mM NaCl, 0.1% Tween 20) overnight at 4°C and subsequently incubated with primary anti-SMN antibodies (BD Transduction Laboratories), followed by washing and incubation with horseradish peroxidase-conjugated goat anti-mouse immunoglobulin G (Jackson Immunoresearch). For a loading control, membranes were stripped with buffer containing 10 mM Tris, 75 mM NaCl, 1% sodium dodecyl sulfate, and 10 mM β-mercaptoethanol (30 min at 60°C) and reprobed for α-tubulin. Monoclonal antibodies against α-tubulin were from Sigma. Immunoreactive proteins were visualized with SuperSignal West Dura Extended Duration Substrate (Pierce). The membranes were scanned with a LAS-1000 Image Reader (Fuji Photo Film Inc.). Results were confirmed by three independent experiments.

RESULTS

Identification of a novel ISS. We have previously shown that a weak 5′ ss facilitates exon 7 exclusion in *SMN2* (51). To explore whether an intronic *cis* element contributes to the weak 5′ ss, we generated *SMN2* minigene mutants with different deletions at the 5′ end of intron 7. We then determined the in vivo splicing pattern of these mutants with highly transfectable cell line C33a (Fig. 2B). In all of the deletions, we retained the first nine nucleotides of intron 7. These nucleotides are conserved among mammals and harbor the canonical base-pairing region for U1 snRNA, a component of U1 snRNP. We first chose to make five-nucleotide-long deletions between positions 10 and 34 (mutants N1Δ10–14, N1Δ15–19, N1Δ20–24, N1Δ25–29, and N1Δ30–34; Fig. 2B, lanes 4 to 8). Our analysis revealed two inhibitory stretches, from position 10 to position 14 (CCAGC) and from position 20 to position 24 (GAAAG), separated by a five-nucleotide sequence (AUUAU). Deletion of GAAAG produced the strongest stimulatory effect (mutant N1Δ20–24; Fig. 2B, lane 6), whereas deletion of CCAGC produced a moderate but noticeable stimulatory effect (mutant N1Δ10–14; Fig. 2B, lane 4). Deletion of AUUAU produced no stimulatory effect (mutant N1Δ15–19; Fig. 2B, lane 5), suggesting that this deletion may strengthen an inhibitory element by bringing the flanking sequences CCAGC and GAAAG together. Consistently, when AUUAU was deleted together with either CCAGC or GAAAG, *SMN2* exon 7 inclusion increased (mutants N1Δ10–19 and N1Δ15–24; Fig. 2B, lanes 9 and 10, respectively). In general, 10- or 15-nucleotide deletions that did not include CCAGC or GAAAG produced no stimulatory effect on exon 7 inclusion (mutants N1Δ25–34 and N1Δ25–39; Fig. 2B, lanes 12 and 16, respectively).

The above results support the presence of a negative element downstream of the U1 snRNA binding site in intron 7 between positions 10 and 24. We call it ISS-N1. To confirm that the stimulatory effect of ISS-N1 deletion was not due to the creation of an enhancer element, we made two additional 20- and 25-nucleotide-long deletions. Both deletions included the complete ISS-N1 sequence (mutants N1Δ10–29 and N1Δ10–34; Fig. 2A). Similar to ISS-N1 deletion (mutant N1Δ10–24), they restored exon 7 inclusion in *SMN2* to the level of *SMN1* (Fig. 2B, lanes 17 and 18). In all three mutants (N1Δ10–24, N1Δ10–29, and N1Δ10–34), the nature of the sequences downstream of the U1 snRNA binding site was different, suggesting that exon 7 inclusion was not due to the gain of a specific *cis* element but due to the loss of ISS-N1.

To determine whether ISS-N1-mediated downregulation of exon 7 inclusion in *SMN2* is tissue specific, we used five additional cell lines that included human SK-N-SH, HEK-293, mouse Neuro-2a, mouse P19, and mouse NSC-34 cells. These cell lines were transfected with the ISS-N1-deleted *SMN2* minigene (mutant N1Δ10–24 in Fig. 2A). Hereafter, we refer to mutant N1Δ10–24 as SMN2ΔISS-N1. Similar to the cervical carcinoma cell line C33a (Fig. 2B), all cell types supported exon 7 inclusion in SMN2ΔISS-N1 (Fig. 2C). Our results suggest that ISS-N1-mediated suppression of *SMN2* exon 7 inclusion is not specific to a particular cell type.

ISS-N1 is absent in mouse *Smn*. In contrast to humans, mice have a single *Smn* gene, which is equivalent to human *SMN1*. Alignment of human and mouse introns 7 showed three sub-

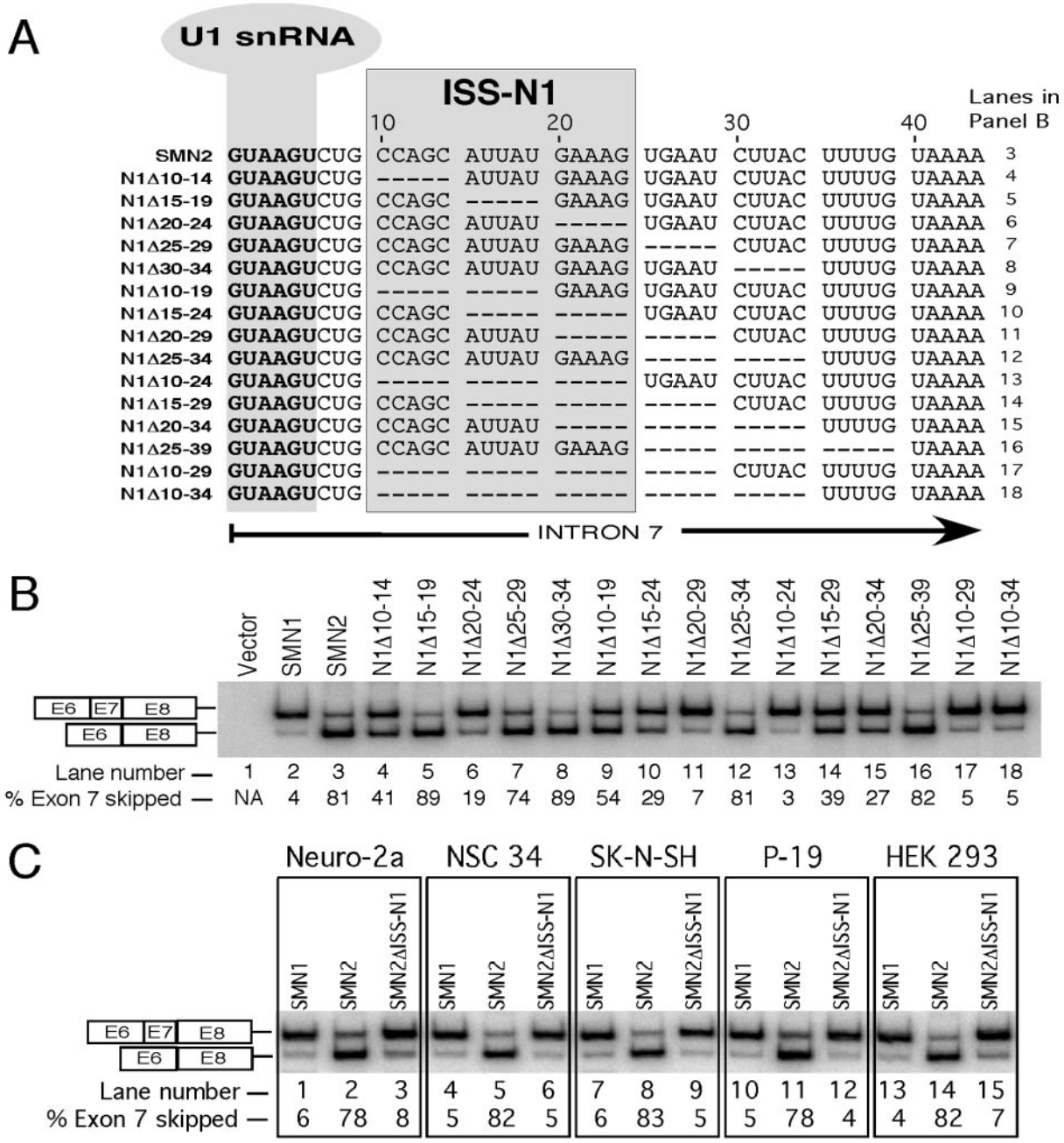

FIG. 2. Effects of intronic deletions downstream of the 5′ ss of exon 7 of *SMN2*. (A) Intronic sequences of *SMN2* deletion mutants. Nucleotide numbering starts from the beginning of intron 7. Deletions are shown as dashed lines. The ISS-N1 site is shaded. Nucleotides involved in base pairing with U1 snRNA are in bold and shaded. Numbers in mutants' names represent the positions at which deletions were made. (B) In vivo splicing pattern of *SMN2* deletion mutants shown in panel A. The upper band corresponds to a fully spliced product that includes exon 7; the lower band corresponds to an exon 7-skipped product. The percentage of exon 7 skipping was calculated from the total value of exon 7-included and exon 7-skipped products. Abbreviations E6, E7, and E8 stand for exon 6, exon 7, and exon 8, respectively. (C) In vivo splicing pattern of SMN2ΔISS-N1 (ISS-N1-deleted mutant) in different cell lines. Of note, SMN2ΔISS-N1 is the same construct as the N1Δ10–24 mutant in panel A. Cell lines used were Neuro-2a (mouse brain neuroblastoma, lanes 1 to 3), NSC-34 (mouse motor neuron like, lanes 4 to 6), SK-N-SH (human neuroblastoma, lanes 7 to 9), P-19 (mouse embryonic teratocarcinoma, lanes 10 to 12), and HEK-293 (lanes 13 to 15). Spliced products are the same as those indicated in panel B. NA, not applicable.

stitutions and three deletions in the ISS-N1 region of mouse intron 7 (Fig. 3A). There are also four additional substitutions in the 15-nucleotide-long stretch following ISS-N1. To test whether differences between human and mouse intronic sequences affect splicing of exon 7, we exchanged the ISS-N1 region of our *SMN2* minigene for the mouse sequence by introducing three substitutions and three deletions (mutant SMN2/MS8, Fig. 3A). This *SMN2* mutant displayed full resto-

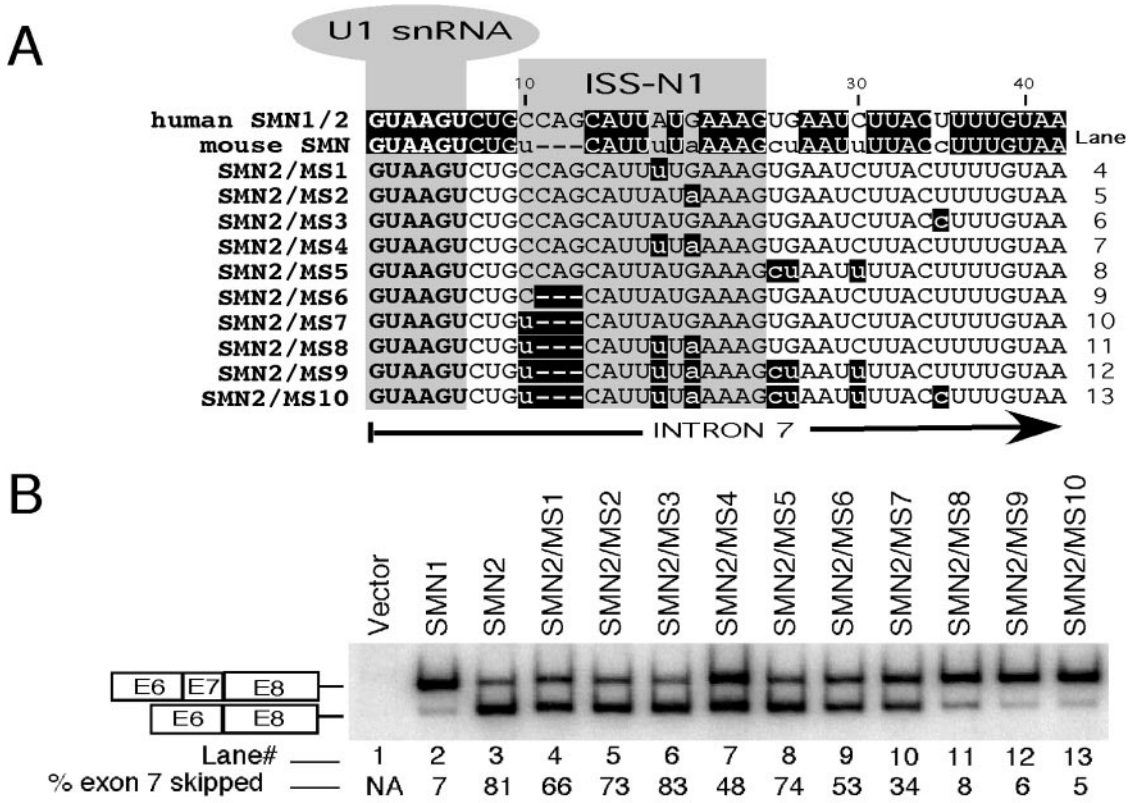

FIG. 3. Evolutionary significance of ISS-N1. (A) Alignment of the first 42 nucleotides of human and mouse introns 7, including the ISS-N1 region. Numbering starts from the beginning of intron 7. ISS-N1 is shaded. Nucleotides involved in base pairing with U1 snRNA are in bold and shaded. In the top two lines, positions homologous between the human and mouse sequences are shaded in black. In the bottom 10 lines, intronic sequences of *SMN2* mutants (SMN2/MS1 through SMN2/MS10) are shown with mouse nucleotides written in lowercase letters and shaded in black. (B) In vivo splicing pattern of *SMN2* mutants shown in panel A. Spliced products are the same as those indicated in Fig. 2B. NA, not applicable.

ration of exon 7 inclusion (Fig. 3B, lane 11). To further dissect the role of acquired mutations within ISS-N1, we tested the splicing pattern of *SMN2* mutants that incorporated different combinations of deletions and substitutions corresponding to mouse sequences. Consistent with the inhibitory role of acquired mutations, a single A18U substitution in the middle of ISS-N1 increased exon 7 inclusion in *SMN2* from ~19% to ~34% (mutant SMN2/MS1, Fig. 3B, lane 4). When A18U was combined with G20A, the exon 7 inclusion increased to ~50% (mutant SMN2/MS4, Fig. 3B, lane 7). A triple deletion from position 11 to position 13 accounted for an increase of ~28% (from 19% to 47%) (mutant SMN2/MS6, Fig. 3B, lane 9). When this triple deletion was combined with an adjacent C10U substitution, exon 7 inclusion increased to ~66% (mutant SMN2/MS7, Fig. 3B, lane 10). As a control, we made substitutions within sequences downstream of ISS-N1. Contrary to the mutations within ISS-N1, the effects of these substitutions were negligible (mutants SMN2/MS3 and SMN2/MS5, Fig. 3B, lanes 6 and 8, respectively). These results are in full agreement with the results of deletion mutations that defined the approximate boundary of ISS-N1 in human intron 7 (Fig. 2A and B).

Antisense oligonucleotide validates the inhibitory role of ISS-N1. To further confirm the presence of inhibitory element ISS-N1, we designed a series of antisense oligonucleotides (ribo-oligonucleotides) that were complementary to intronic sequences downstream of the U1 snRNA binding site, including the ISS-N1 region. Antisense oligonucleotide Anti-N1 fully blocked ISS-N1 by annealing to a 20-nucleotide-long sequence starting from position 10 of intron 7 (Fig. 4A). Antisense oligonucleotide Anti-N1+10 partially targeted ISS-N1 by annealing to a sequence starting from position 20 of intron 7 (Fig. 4A). Anti-N1+20 and Anti-N1+30 annealed to sequences downstream of ISS-N1 starting from positions 30 and 40, respectively (Fig. 4A). To increase the intracellular stability of oligonucleotides, all of them had a phosphorothioate backbone and a 2′-*O*-methyl modification in the sugar moiety. Antisense oligonucleotides with similar modifications have been used to correct aberrant splicing in vivo (10, 33). The effect of antisense oligonucleotides on *SMN2* splicing was determined by cotransfection of C33a cells with 1.0 μg of the *SMN2* minigene and 50 nM antisense oligonucleotides. Consistent with the result obtained with deletion mutant N1Δ10–29 (Fig. 2B), Anti-N1 restored exon 7 inclusion in *SMN2* to the level of *SMN1* (Fig. 4B, lane 4). Complete restoration of *SMN2* exon 7 inclusion was also observed at Anti-N1concentrations as low as 10 nM when the amount of the *SMN2* minigene was reduced to 0.1 μg (not shown). Three other antisense oligonucleotides that annealed to the downstream sequences did not produce any stimulatory effect (Fig. 4B, lanes 5 to 7). The results de-

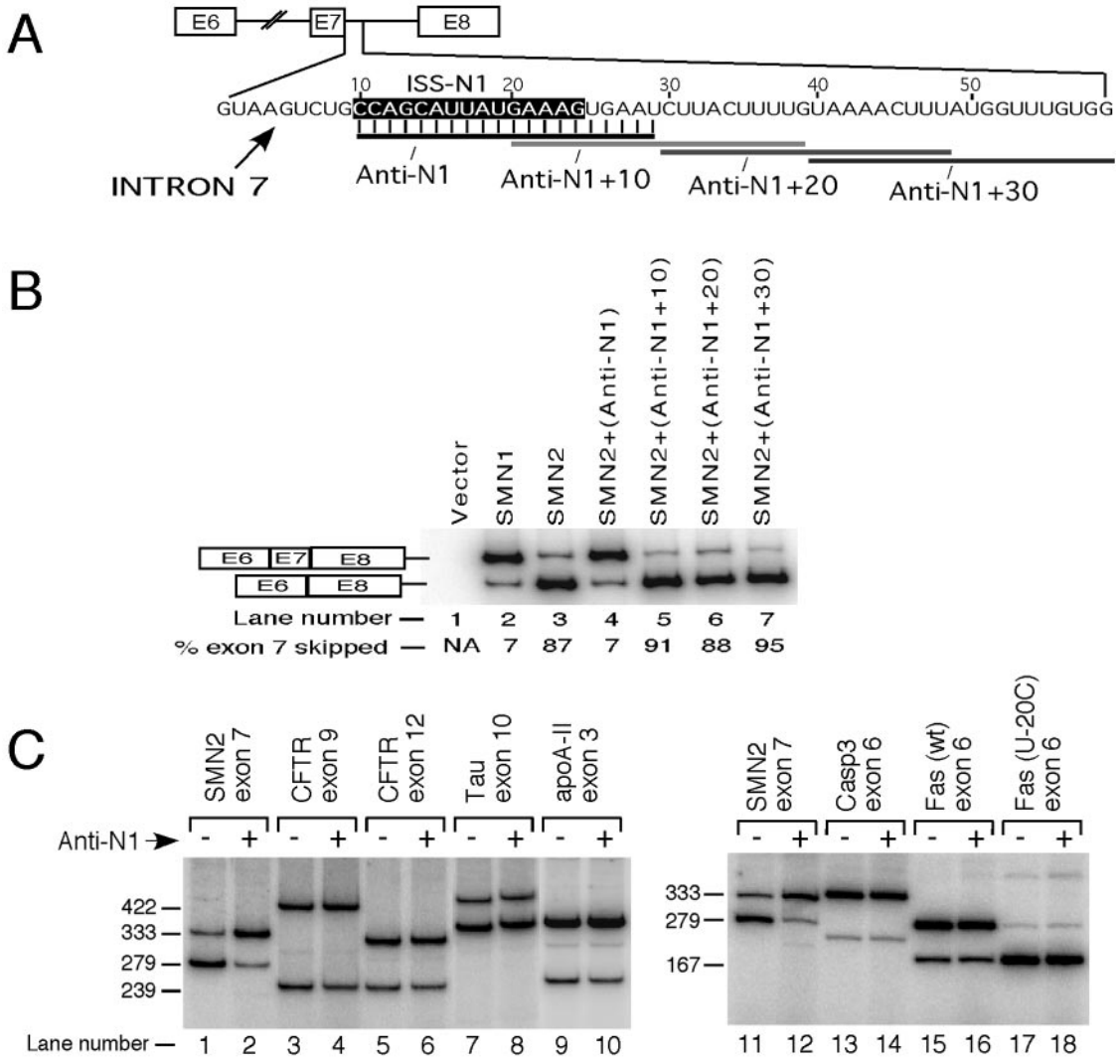

FIG. 4. Effects of antisense oligonucleotides on splicing of different minigenes. (A) Diagrammatic representation of intron 7 regions targeted by antisense oligonucleotides Anti-N1, Anti-N1+10, Anti-N1+20, and Anti-N1+30. Numbering starts from the beginning of intron 7. The ISS-N1 region is shaded. Of the four oligonucleotides shown, only Anti-N1 fully sequestered ISS-N1. (B) In vivo splicing pattern of the *SMN2* minigene in the presence of antisense oligonucleotides. Spliced products are the same as those indicated in Fig. 2B. (C) In vivo splicing pattern of different minigenes in the presence of Anti-N1. In every lane, the upper band represents the exon-included and the lower band represents the exon-excluded products. In *CFTR*, *apoA-II*, *Fas*, and *Casp3*, the major bands represent the exon-included products. In *Tau* and *Fas* (U-20C), the major bands represent the exon-excluded products. For detection of spliced products in lanes 1 to 6, 9, and 10, cells were harvested 40 h after transfection (for other lanes, see Materials and Methods). The values on the left are sizes in base pairs. wt, wild type; NA, not applicable.

scribed were reproducible with two different batches of antisense oligonucleotides synthesized at different times.

To confirm that Anti-N1 does not have a nonspecific effect on alternative splicing of other exons, we performed the following experiment. C33a cells were transfected with different minigenes in the presence and absence of Anti-N1, and in vivo splicing patterns were determined. These minigenes were randomly selected and represented a good mixture of exon-including and exon-excluding cassettes (Fig. 4C). Among the minigenes that showed low skipping of exons were pTBEx9-V456F (~25% skipping of *CFTR* exon 9), pTBEx12-50A (~20% skipping of *CFTR* exon 12), pTBApo-ISE3m (~15% skipping of *apoA-II* exon 3), *Casp3* (~6% skipping of *Caspase 3* exon 6), and CMV-Fas (wt) (~6% skipping of *Fas* exon 6). Among the minigenes that showed mostly skipping of exons were SI9/LI10 (~85% skipping of *Tau* exon 10) and CMV-Fas (U-20C) (~98% skipping of *Fas* exon 6). In the above experiments, we used 50 nM Anti-N1 while the minigene-containing plasmid concentration was decreased to 0.1 μg. A high Anti-N1-to-minigene ratio was deliberately chosen to detect the nonspecific effect at the nonlimiting Anti-N1 concentration. Underscoring the specificity of Anti-N1 for *SMN* intron 7, we did not notice an appreciable change in the splicing pattern of any of the minigenes cotransfected with Anti-N1 (Fig. 4C).

The stimulatory effect of Anti-N1 is caused by base pairing with the target sequence. To prove that the stimulatory effect of Anti-N1 was solely due to blocking of ISS-N1, we performed cotransfection experiments with *SMN2* minigenes that had ran-

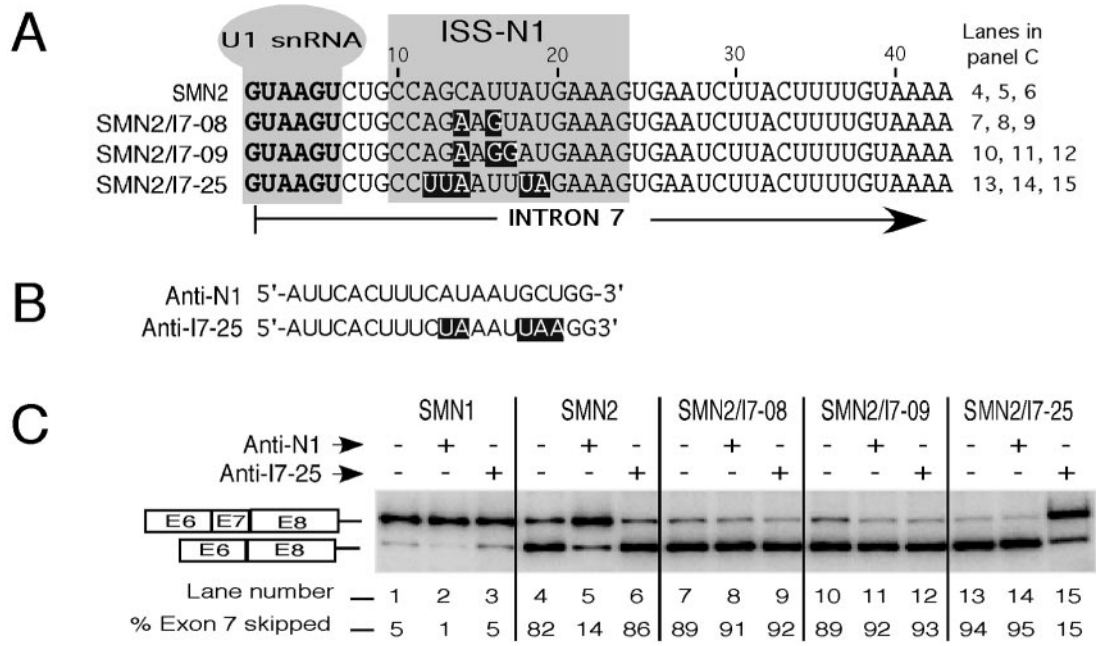

FIG. 5. Effect of base pairing between Anti-N1 and ISS-N1 on the efficiency of *SMN2* exon 7 inclusion. (A) Intron 7 sequences of *SMN2* and mutants with substitutions in the ISS-N1 region. Numbering starts from the beginning of intron 7. The ISS-N1 region is shaded in gray. Nucleotides involved in base pairing with U1 snRNA are in bold and shaded. Note that intronic mutations (shaded in black) abrogate base pairing between Anti-N1 and ISS-N1. (B) Sequences of Anti-N1 and Anti-I7-25 oligonucleotides. Differences are shaded in black. Note that Anti-I7-25 restores base pairing with the ISS-N1 region in mutant SMN2/I7-25. (C) In vivo splicing pattern of mutants shown in panel A. Plasmid DNA (0.1 μg) was transfected alone or cotransfected with 50 nM Anti-N1 or Anti-I7-25 oligonucleotide. Spliced products are the same as those indicated in Fig. 2B.

dom mutations within ISS-N1 (Fig. 5A). Of note, from a large library of ISS-N1 mutants, we chose only those in which substitutions did not affect *SMN2* exon 7 inclusion but abrogated base pairing between ISS-N1 and Anti-N1. Consequently, upon cotransfection, Anti-N1 did not stimulate exon 7 inclusion in any of these mutants (Fig. 5C). Remarkably, the stimulatory effect of Anti-N1 completely disappeared even with a mutant that had only a 2-bp mismatch with Anti-N1 (Fig. 5C, lanes 7 and 8). Noticeably, Anti-N1 also reduced *SMN1* exon 7 exclusion from ~5% to ~1% (Fig. 5C, compare lane 1 with lane 2), suggesting that blocking of ISS-N1 has the potential to upregulate SMN expression from both *SMN1* and *SMN2*.

To further confirm that the observed antisense oligonucleotide-mediated stimulatory effect was due to base pairing between the antisense oligonucleotide and ISS-N1, we included a mutant oligonucleotide in our cotransfection experiments (Anti-I7-25, Fig. 5B and C). This oligonucleotide formed perfect base pairing with the ISS-N1 region of the SMN2/I7-25 minigene. We chose to target the SMN2/I7-25 construct deliberately since its ISS-N1 region contains five substitutions (a 33% change that includes a more-than-twofold increase in U residues and a 33% decrease in G residues in 15-nucleotide-long ISS-N1). Therefore, by using Anti-I7-25 we were able to test the effect of base pairing in the mutant that retains inhibitory function despite a major change in the sequence composition. Remarkably, Anti-I7-25 produced an about sixfold increase in exon 7 inclusion in SMN2/I7-25 (Fig. 5C, lane 15). At the same time, Anti-I7-25 had no stimulatory effect on the splicing pattern of the *SMN1* or *SMN2* minigene. Similarly, Anti-I7-25 did not affect the splicing pattern of mutants SMN2/I7-08 and SMN2/I7-09. The above results conclusively confirm the inhibitory role of ISS-N1 and demonstrate that the antisense oligonucleotides produce specific stimulatory effects on exon 7 inclusion when ISS-N1 is blocked by base pairing.

Deletion of ISS-N1 rescues exon 7 inclusion in mutants with abrogated positive *cis* elements. To assess the relative impact of ISS-N1 on exon 7 splicing, we generated *SMN1* mutants in which ISS-N1 deletion was combined with abrogation of one of the stimulatory *cis* elements. In particular, we tested the impact of ISS-N1 deletion on inhibitory substitutions within four positive *cis* elements, i.e., intronic element 2 (39, 40), Tra2-ESE (18), Conserved tract (51), and a critical guanosine residue at the first position of exon 7 (50, 51). A diagrammatic representation of the relative positioning of these elements is shown in Fig. 6A. Demonstrating the cross-exon effect, deletion of ISS-N1 fully restored exon 7 inclusion in *SMN1* harboring a guanosine-to-uridine substitution at the first position of exon 7 (mutant SMN1ΔISS-N1/1U, Fig. 6B, lane 9). Similarly, deletion of ISS-N1 promoted exon 7 inclusion in *SMN1* mutants with abrogated element 2 (mutant SMN1ΔISS-N1/Abr-E2, Fig. 6B, lane 8) and abrogated Tra2-ESE (mutant SMN1ΔISS-N1/Abr-Tra2, Fig. 6B, lane 10). Although less prominent, the stimulatory effect of ISS-N1 deletion was clearly detectable in an *SMN1* mutant with an abrogated Conserved tract (mutant SMN1ΔISS-N1/Abr-CT, Fig. 6B, lane 11). These results demonstrate for the first time that a single intronic element has such a strong impact on exon 7 splicing in *SMN* genes.

ISS-N1 shows portability within *SMN2* intron 7, as well as in a heterologous system. To demonstrate the portability of ISS-N1 within intron 7, we generated four mutants in which

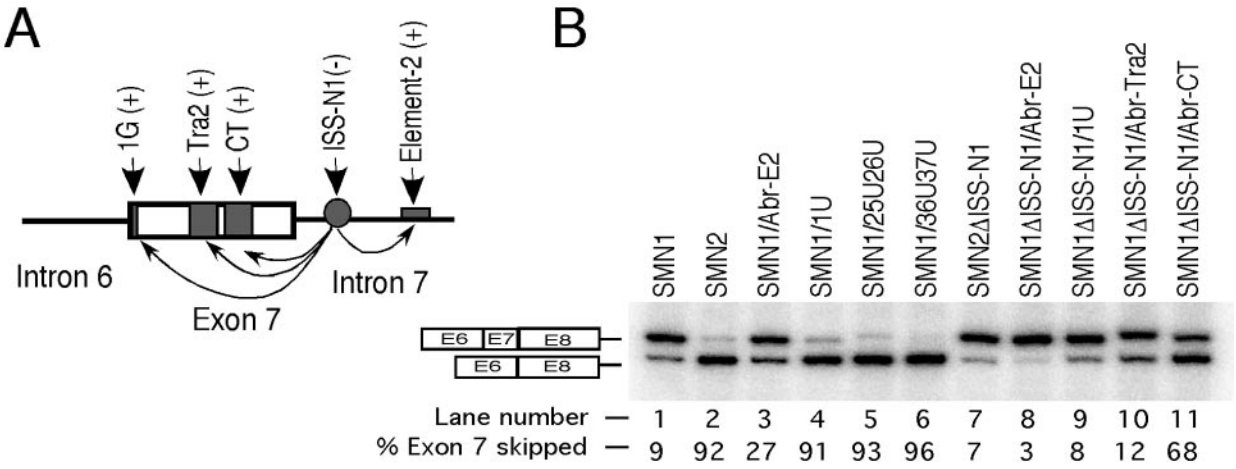

FIG. 6. Relative significance of exon 7 *cis* elements vis-à-vis ISS-N1. (A) Diagrammatic representation of several *cis* elements involved in regulation of exon 7 splicing (not to scale). 1G, Tra2-β1 (Tra2-ESE), CT (Conserved tract), and element 2 represent positive elements (+). ISS-N1 is a negative element (−). (B) In vivo splicing pattern of *SMN1* mutants in which deletion of ISS-N1 (ΔISS-N1) was combined with abrogation of a given positive *cis* element. Spliced products are the same as those indicated in Fig. 2B. Abr-E2 represents abrogation of element 2 by a triple substitution G69C/U70A/U71A in intron 7 (40), Abr-Tra2 represents abrogation of Tra2-ESE by a 25U26U mutation in exon 7 (18), 1U mutation represents abrogation of a *cis* element at the first position (51), and Abr-CT represents abrogation of Conserved tract by a 36U37U mutation in exon 7 (51).

ISS-N1 was moved away from the 5′ ss of *SMN2* exon 7 (Fig. 7A, top). We then tested the splicing pattern of these mutants. While moving ISS-N1 five nucleotides away from its original position fully retained the inhibitory impact of ISS-N1 (Fig. 7B, lane 3), there was a little decrease in the inhibitory effect (from ~89% to ~72%) when ISS-N1 was moved another five nucleotides (Fig. 7B, lane 4). Moving of ISS-N1 20 nucleotides away from its original position produced a dramatic effect in which exon 7 exclusion decreased from ~89% to ~18% (Fig. 7B, lane 5). Further moving of ISS-N1 by another 15 nucleotides completely eliminated the inhibitory impact of ISS-N1 and restored exon 7 inclusion in *SMN2* to the level of *SMN1* (Fig. 7B, lane 6). These results demonstrate the limited portability of ISS-N1 in which the inhibitory effect of ISS-N1 seems to be tied to its close proximity to the 5′ ss.

The observation that moving ISS-N1 five nucleotides away from its original position fully retained the inhibitory impact of ISS-N1 (mutant ISS-N1-M5 in Fig. 7A) suggests that the nature of the five-nucleotide-long sequence UGAAU that immediately precedes ISS-N1 was unable to break the inhibitory context responsible for the ISS-N1-mediated exclusion of exon 7. To determine whether the ISS-N1-associated inhibitory impact is context specific, we examined the effects of five-nucleotide-long insertions immediately preceding ISS-N1 (Fig. 7A, bottom). Insertion of five guanosine residues that created an eight-nucleotide-long GC-rich stretch upstream of ISS-N1 did not change exon 7 splicing in *SMN2* (Fig. 7B, lane 12). Similarly, insertion of five adenosines upstream of ISS-N1 had a negligible effect on the splicing pattern of *SMN2* (Fig. 7B, lane 9). Insertion of five C residues created a stretch of seven cytosines and partially improved exon 7 inclusion in *SMN2* (Fig. 7B, lane 11). However, insertion of five uridines alleviated the inhibitory effect of ISS-N1 and substantially increased *SMN2* exon 7 inclusion (Fig. 7B, lane 10). These results suggest that the inhibitory impact of the ISS-N1 element is not only dependent upon the proximity of ISS-N1 to the 5′ ss but is also intimately connected to the nature of sequences immediately upstream of ISS-N1. As controls, we tested the impact of identical insertion mutations in *SMN1*. Underscoring that these insertions have no independent inhibitory effect, none of these mutations affected *SMN1* exon 7 splicing (Fig. 7B, lanes 13 to 17).

Having demonstrated the limited portability of ISS-N1 within intron 7 of *SMN2*, we decided to check the portability of ISS-N1 in a heterologous context, with a *Casp3* minigene that contains the *Caspase 3* genomic sequence from exon 5 through exon 7. This minigene recapitulates the partial skipping of endogenous *Caspase 3* exon 6 reported by Huang et al. (21). Insertion of an AvrII restriction site downstream of exon 6 did not change the splicing pattern of exon 6 (compare lane 1 in Fig. 7D with lane 13 in Fig. 4C) but allowed us to insert ISS-N1 for testing the portability of this element in a heterologous context. As shown in Fig. 7C, we inserted the ISS-N1 sequence nine nucleotides away from the 5′ ss of exon 6 (mutant Casp3ISS-N1, Fig. 7C). We deliberately chose this position because ISS-N1 is located at the identical position within intron 7 of *SMN* genes (Fig. 2A). Interestingly, ISS-N1 insertion caused an about sixfold increase in skipping of *Casp3* exon 6 (Fig. 7D, compare lane 1 with lane 3). Blocking of ISS-N1 by a 15-nucleotide-long antisense oligonucleotide (Anti-ISS-N1/15) fully restored the inclusion of *Casp3* exon 6 (Fig. 7D, compare lane 4 with lane 3). We used the *SMN2* minigene as the positive control for testing the effect of Anti-ISS-N1/15. As expected, Anti-ISS-N1/15 fully restored exon 7 inclusion in transcripts derived from the *SMN2* minigene. The above results confirm that ISS-N1 is a portable inhibitory element even in a heterologous context. Remarkably, ISS-N1 was able to exert its inhibitory impact despite the presence of G residues at the first and last positions of exon 6 in *Casp3* (Fig. 7C). We have previously shown that the presence of a G residue at the

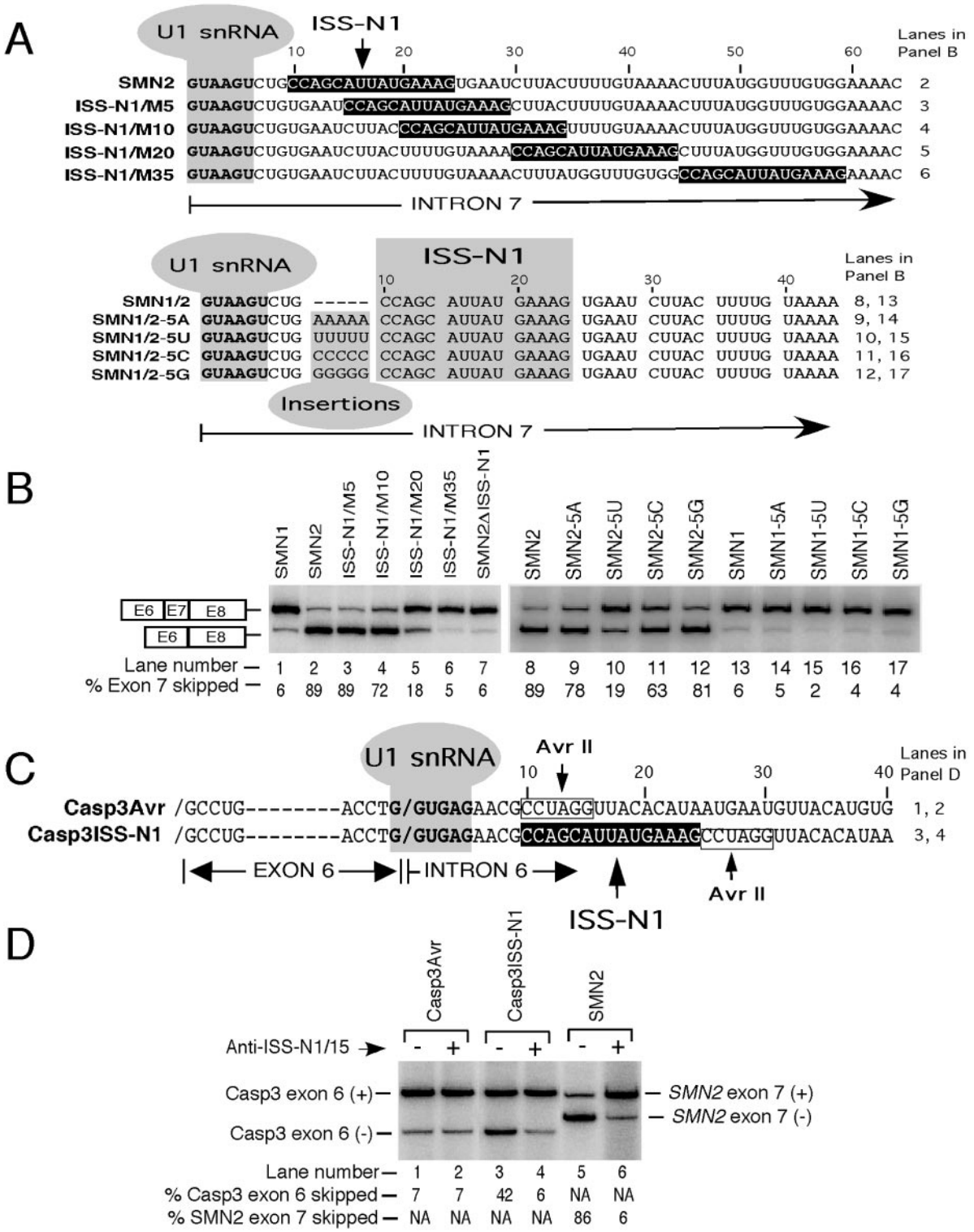

FIG. 7. Portability of ISS-N1. (A, top) Location of ISS-N1 within *SMN2* intron 7 with respect to the 5′ ss. ISS-N1 was inserted at different locations within intron 7 of SMN2ΔISS-N1. (A, bottom) Intronic sequences of *SMN2* mutants with five-nucleotide-long insertions immediately upstream of ISS-N1. Nucleotide positions and types of insertions are indicated. Numbering starts from the beginning of intron 7. ISS-N1 is shaded. Nucleotides involved in base pairing with U1 snRNA are in bold and shaded. (B) In vivo splicing pattern of mutants shown in panel A. Spliced products are the same as those indicated in Fig. 2B. (C) Insertion of ISS-N1 in a heterologous context. For insertion of ISS-N1, an AvrII restriction site was first inserted downstream of exon 6 of the *Casp3* minigene. (D) In vivo splicing pattern of mutants shown in panel C. The splicing pattern was determined in the absence and presence of an antisense oligonucleotide (Anti-ISS-N1/15) that fully sequesters ISS-N1. In the absence of Anti-ISS-N1/15, the Casp3ISS-N1 mutant increases exclusion of *Casp3* exon 6 (compare lane 3 with lane 4). NA, not applicable.

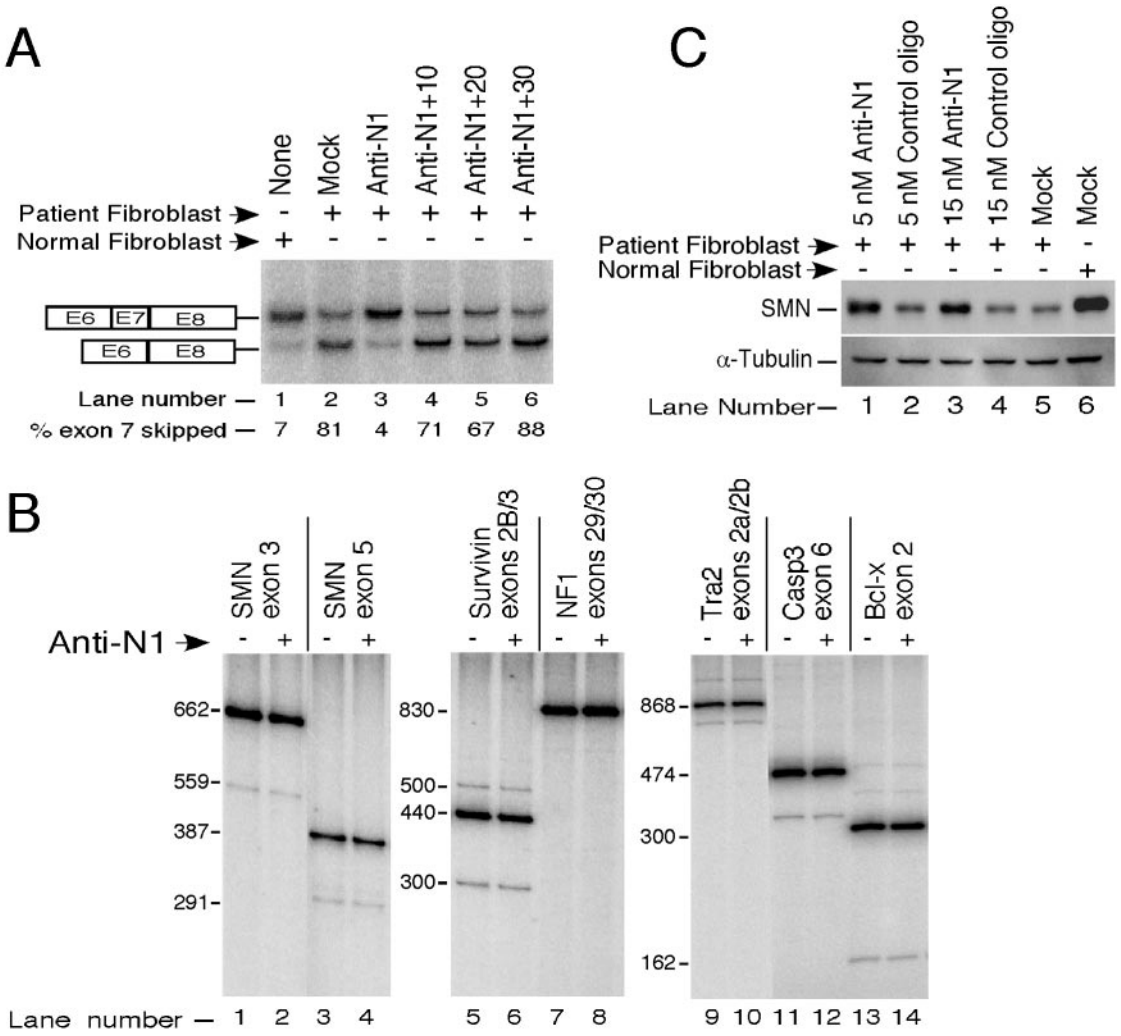

FIG. 8. Effect of Anti-N1 on the splicing of endogenous genes. (A) Splicing of endogenous *SMN2* after SMA fibroblasts (GM03813) were transfected with 5 nM oligonucleotides. Total RNA was collected 25 h after transfection. (B) Specificity of the effect of Aniti-N1 on the splicing pattern of other exons in SMA fibroblasts (GM03813). The sizes of the expected spliced products are indicated on the left. The same RNA as that used in panel A (lanes 2 and 3) was used for analysis. The 662-bp bands in lanes 1 and 2 represent the *SMN* exon 3-included product, and the 387-bp bands in lanes 3 and 4 represent the *SMN* exon 5-included product. The 440-bp bands in lanes 5 and 6 represent transcripts that exclude exon 2b but include exon 3 of *Survivin* (34). The 830-bp bands in lanes 7 and 8 represent transcripts that include exons 29 and 30 of *NF1* (48). The 686-bp bands in lanes 9 and 10 represent transcripts that produce a Tra2-β1 spliced variant of *Tra2* (8). The 474-bp bands in lanes 11 and 12 represent the *Caspase 3* exon 6-included product (21). The 300-bp bands in lanes 13 and 14 represent a Bcl-xL spliced variant of *Bcl-x* (37). (C) Effect of Aniti-N1 on the level of SMN protein. Western blotting was performed to detect SMN in SMA fibroblasts (GM03813) transfected with 5 nM (lane 1) and 15 nM (lane 3) Anti-N1. GM03813 cells transfected with control oligonucleotide Scramble20 (lanes 2 and 4) and mock-transfected GM03813 cells (lane 5) or AG06814 cells (normal fibroblasts) (lane 6) were used as controls. For detection of SMN, cells were harvested 72 h after transfection. We used α-tubulin as a loading control. The values on the left are sizes in base pairs.

last position of exon 7 in *SMN2* renders exon 7 exclusion undetectable even in a sensitive radioactive assay (51).

Anti-N1 corrects the aberrant splicing of endogenous *SMN2* and increases SMN protein in SMA cells. Since the studies described above were performed with *SMN* minigenes, we decided to validate the inhibitory activity of ISS-N1 in the context of endogenous *SMN2*. The SMA type I fibroblast line GM03813 carries the entire *SMN2* but no *SMN1*. Accordingly, these cells produce high levels of exon 7-excluded products (Fig. 8A, lane 2). As expected, transfection of GM03813 cells (SMA cells) with increasing concentrations of Anti-N1 yielded increased exon 7 inclusion (not shown). The minimum concentration at which the level of exon 7 inclusion in SMA cells increased to the level observed in normal fibroblasts was 5 nM. Consequently, we transfected SMA cells with 5 nM antisense oligonucleotides (Anti-N1, Anti-N1 + 10, Anti-N1 + 20, and Anti-N1 + 30). The annealing positions of the above oligonucleotides are the same as those shown in Fig. 4A. Only Anti-N1 restored exon 7 inclusion in SMA cells comparable to that of normal fibroblasts (Fig. 8A). Three other oligonucleotides produced no appreciable stimulatory effects (Fig. 8A). The experiments were reproducible with two batches of oligonucleotides. These results validate the inhibitory role of ISS-N1 in the context of an endogenous *SMN2* transcript.

To confirm that Anti-N1 does not cause aberrant splicing of other exons in patient cells, we performed the following experiment. RNA preparations from untreated fibroblasts and fibroblasts treated with 5 nM Anti-N1 (Fig. 8A, lanes 2 and 3) were used to determine the splicing pattern of a limited number of the randomly selected endogenous genes that are known to generate alternatively spliced products (8, 21, 34, 37, 48). We did not find a detectable change in the splicing pattern of any of the examined genes, including *Tra2*, which produces Tra2-β1 (compare the 868-bp bands in lanes 9 and 10 in Fig. 8B) (8). Tra2-β1 plays a stimulatory role in *SMN2* exon 7 inclusion but is downregulated in SMA patient cells (17). Also, the splicing pattern of *SMN* exons 3 and 5 remained unaffected in patient cells treated with Anti-N1. These exons have been shown to undergo alternative splicing (20). Despite the small sample size, our results do not support a global adverse effect of Anti-N1 on the alternative splicing of other genes.

To demonstrate that Anti-N1-mediated blocking of ISS-N1 leads to increased levels of SMN protein, we treated SMA cells with 5 or 15 nM Anti-N1. These concentrations fall within the lower range of Anti-N1 concentrations that corrected *SMN2* splicing in patient cells. Both concentrations caused a significant increase in the SMN protein level (Fig. 8C). This is the first report of a study in which an antisense oligonucleotide-assisted increase in the level of SMN protein in patient cells was detected by Western blotting. This may have been possible due to a more-than-fivefold increase in exon 7 inclusion from the endogenous *SMN2* minigene (Fig. 8A). The level of SMN protein remained elevated for 5 days after transfection. To confirm the specificity of Anti-N1-induced stimulation, we used a scrambled oligonucleotide as a negative control. As shown in Fig. 8C (lanes 2 and 4), this oligonucleotide did not produce any detectable increase in the levels of SMN protein.

DISCUSSION

Alternative pre-mRNA splicing is a complex event in which *cis* elements located in both exonic and intronic sequences play an important role. Compared to exonic *cis* elements, the role of intronic *cis* elements in the modulation of alternative splicing is poorly understood (54). Further, there are no algorithms to accurately predict intronic *cis* elements. The task of identifying intronic *cis* elements is also complicated by the large size of introns. Here we describe a novel intronic *cis* element, ISS-N1 (CCAGCAUUAUGAAAG), which is located in the nonconserved portion of the final intron (intron 7) of human *SMN*. This element was found to be an important component of a regulatory network that modulates alternative splicing of *SMN* exon 7, which is linked to the pathogenesis of SMA.

We began this study as a follow-up to one of the important findings of our in vivo selection: a weak 5′ ss is the dominant cause of exon 7 exclusion in *SMN2* (51). Consistently, we demonstrated that exonic sequences near the 5′ ss of exon 7 form an inhibitory element called 3′-Cluster. Interestingly, 3′-Cluster was found to overlap sequences that are not conserved among mammals, suggesting an evolutionary constraint in which a novel regulatory network evolved just before the duplication of *SMN*. Such an arrangement may even have favored *SMN* duplication as SMN expression was already under the tight control of inhibitory *cis* elements that rendered the 5′ ss of exon 7 poorly accessible. We reasoned that the nonconserved intronic sequences might have played a key role in creating a poorly accessible 5′ ss. Thus, we analyzed a series of deletion mutations within adjacent intron 7. This led to the identification of ISS-N1, an inhibitory *cis* element located immediately downstream of the 5′ ss in intron 7 of human *SMN* genes (Fig. 2).

The observation that substitutions in the nonconserved portions of intron 7 restore exon 7 inclusion in *SMN2* reveals the significance of noncoding sequences that acquired an additional function during evolution to downregulate SMN expression (Fig. 3). Our results support a hypothesis that human-specific alternative splicing of exons may be linked to the evolutionarily divergent intronic sequences. Interestingly, the sequence between positions 7 and 30 of intron 7 was found to be more conserved (~67%) than expected (~55%) based on the statistical prevalence of conserved residues between the human and mouse intronic sequences downstream of a constitutively spliced exon (54). This underscores that the type of mutations, not their number, played a significant role in creating novel *cis* elements during evolution. It is not known if the mouse sequence that corresponds to ISS-N1 contains an enhancer element that is recognized by a splicing factor. Interestingly, this region in the mouse contains a UUUAA motif, which has been found to be a winning pentamer within low G+C content intronic sequences downstream of the 5′ ss (62). Winning pentamers supposedly regulate splicing by an as yet unknown mechanism. Since an ISS-N1-deleted mutant promoted exon 7 inclusion in all cell lines, including mouse cells, we conclude that tissue-specific factors are not involved in ISS-N1-mediated regulation of alternative splicing of exon 7 (Fig. 2C). These results also demonstrate how the relatively conserved pre-mRNA processing machinery uses nonconserved intronic *cis* elements to achieve human-specific regulation.

We used an antisense oligonucleotide-based approach to conclusively demonstrate the inhibitory nature of ISS-N1 (Fig. 4). In this approach, the ISS-N1 sequence was blocked by antisense oligonucleotide Anti-N1. As expected, Anti-N1 fully restored exon 7 inclusion in the *SMN2* minigene. The positive effect of Anti-N1 was very specific to *SMN* exon 7, as no off-target effect on alternative splicing was observed in a comprehensive test that used eight other minigenes (Fig. 4C). In addition, we found that the Anti-N1-mediated stimulatory effect is exclusively dependent upon base pairing with the target (Fig. 5). Consistently, a mutant oligonucleotide (Anti-I7-25) that restored base pairing with a mutated form of ISS-N1 (SMN2/I7-25) also promoted exon 7 inclusion in *SMN2*. Since both deletion of ISS-N1 and substitutions within ISS-N1 promoted exon 7 inclusion in *SMN2* (Fig. 2 and 3), we conclude that antisense oligonucleotide-mediated stimulation of exon 7 inclusion is due solely to blocking of ISS-N1 and not to a nonspecific effect of an RNA-RNA duplex which is formed by annealing of Anti-N1 to ISS-N1. The fact that antisense oligonucleotides that annealed to sequences downstream of ISS-N1 produced no changes in the splicing pattern (Fig. 4B) also rules out the possibility of any stimulatory effect merely due to a double-stranded RNA.

The observation that deletion of ISS-N1 compensates for a number of abrogated stimulatory *cis* elements suggests that

ISS-N1 plays a critical role in alternative splicing of exon 7. ISS-N1 is strategically placed in the vicinity of the 5′ ss, which is poorly defined for several reasons, including poor base pairing with U1 snRNA, a component of U1 snRNP. Consistently, we have previously demonstrated that a single nucleotide substitution (A54G) that increased base pairing between the 5′ ss and U1 snRNA from six to eight nucleotides promoted exon 7 inclusion in *SMN2* (51). Interestingly, we found a striking similarity between the stimulatory effects produced by the A54G mutation and the ISS-N1 deletion. In both cases, exon 7 inclusion was restored despite the abrogation of a number of positive *cis* elements. These results support a very tight control by which the 5′ ss of *SMN* exon 7 is recognized. One of the possible mechanisms by which ISS-N1 exerts its inhibitory impact may involve rendering the 5′ ss inaccessible for the recruitment of U1 snRNP. Consistently, moving ISS-N1 away from the 5′ ss promoted exon 7 inclusion in *SMN2*.

The splicing pattern of *SMN2* mutants in which ISS-N1 was moved 5 or 10 nucleotides away from its original location demonstrated the portability of ISS-N1. These mutations also delineated the 5′ and 3′ boundaries of ISS-N1 and confirmed that intronic sequences immediately upstream and downstream of ISS-N1 are not associated with the inhibitory role of ISS-N1. However, the portability of ISS-N1 was not absolute as moving ISS-N1 20 or 35 nucleotides away from its original location restored exon 7 inclusion in *SMN2*. The limitation of ISS-N1 portability was also revealed by the insertion mutation in which addition of five U residues between the 5′ ss and ISS-N1 substantially increased exon 7 inclusion in *SMN2*. This underscores the specific role of an inhibitory context in which ISS-N1 must cooperate with other negative elements to produce the net effect of exon 7 exclusion during pre-mRNA splicing of *SMN2*. Insertion of U residues may have disrupted this context by creating an enhancer element and/or by providing better accessibility to the 5′ ss through a favorable RNA structure. Consistently, we observed that ISS-N1 was less inhibitory in a heterologous context when it was inserted nine nucleotides away from the 5′ ss of exon 6 of the *Casp3* minigene. However, the impact of ISS-N1 on *Casp3* exon 6 was still greater than that on exon 7 of *SMN1*, which differs from *SMN2* by a critical C6U mutation. This observation highlights how the impact of an intronic *cis* element is altered by exonic mutations that are located more than 60 nucleotides away (C6U in *SMN2* and mutant SMN1/1U in Fig. 6).

Use of antisense oligonucleotide Anti-N1 confirmed the presence of ISS-N1 in the context of the endogenous gene, which is transcribed from a different promoter than the minigene. Further, the endogenous transcript is more than 25-fold larger than the transcript derived from the *SMN2* minigene used in our study. There are several ways in which transcription and the transcript size could affect alternative splicing (1, 26). The fact that blocking of ISS-N1 by low concentrations of Anti-N1 restored exon 7 inclusion in mRNA derived from endogenous *SMN2* demonstrated the feasibility of an intron-interacting oligonucleotide to fully overcome the inhibitory effect of an exonic mutation responsible for producing a truncated protein in patient cells. Such a strong antisense effect is possible only when the antisense target is easily accessible. The strong stimulatory effect of Anti-N1 may also suggest that blocking of ISS-N1 lessens the dependency on exon 7 inclusion-inducing factor Tra2-β1, which is downregulated in SMA (17).

The majority of SMA cases are caused by the deletion of both *SMN1* alleles (28). Fortunately, most patients retain a copy of *SMN2* that could be used to produce the full-length SMN protein. For antisense oligonucleotide-based therapy of SMA, an intronic site is likely to present a better target because an intron-annealed oligonucleotide will not interfere with downstream mRNA metabolism, including exon-junction complex formation, transport, and translation (44). Consistently, we observed increased levels of SMN protein in SMA cells treated with Anti-N1 at a concentration as low as 5 nM. In contrast, a prior study that used a bifunctional oligonucleotide which annealed to exon 7 and required the presence of splicing factor SF2/ASF produced a stimulatory effect on *SMN2* exon 7 inclusion at a concentration of 100 nM (53). Effects on the protein level for other antisense oligonucleotides that promoted exon 7 inclusion in *SMN2* minigenes have not been reported (6, 29, 39).

Antisense oligonucleotide-based therapy might have utility in a number of human diseases associated with aberrant splicing (10, 13, 25, 49). A recent study demonstrated antisense oligonucleotide-mediated correction of aberrant splicing resulting in the restoration of expression of dystrophin in body-wide skeletal muscles of the mouse model of Duchenne muscular dystrophy (33). Mouse models of SMA are available (20, 42). However, for therapeutic applications of antisense oligonucleotides in neuromuscular diseases such as SMA, additional modifications may be required for oligonucleotides to cross the blood-brain barrier. Recent advancements in nucleic acid technology and delivery strategies have broadened the scope of antisense oligonucleotide usage for neuronal disorders (14, 23, 56). Currently, SMA has no therapy. Our discovery of ISS-N1 provides a very specific and accessible intronic target to develop an effective antisense oligonucleotide-based therapy for SMA.

In summary, we have discovered a novel splicing-inhibitory *cis* element, ISS-N1, which is located in the final intron of human *SMN* genes. Deletion of ISS-N1 fully corrected *SMN2* splicing and compensated for the loss of a number of positive splicing elements within *SMN1*. This is the first report demonstrating the profound impact of an intronic *cis* element on alternative splicing of human *SMN* genes. Blocking of ISS-N1 by an antisense oligonucleotide restored exon 7 inclusion in *SMN2* and elevated the levels of SMN protein in SMA patient cells. These findings bring new insights into our understanding of human *SMN* splicing and provide a unique target for correcting the defective gene associated with a devastating disease of infants and children.

ACKNOWLEDGMENTS

We thank Neil Cashman, Juan Valcárce, and Jianhua Zhou for providing NSC-34 cells and the *Fas* and *Tau* minigenes, respectively. We are grateful to Francisco Baralle for providing the *CFTR* and *apoA-II* minigenes. We thank Yening Zhou for making the *Casp3* minigene.

This work was generously supported by grants from Families of SMA (SINR05-06) and the Muscular Dystrophy Association—USA (MDA3969) to R.N.S. N.N.S. and E.J.A. were supported by the National Institutes of Health (R01 NS40275). N.N.S. was also supported by a grant from Families of SMA (SINN05-06).

REFERENCES

1. **Bentley, D. L.** 2005. Rules of engagement: co-transcriptional recruitment of pre-mRNA processing factors. Curr. Opin. Cell Biol. **17:**251–256.
2. **Black, D. L.** 2003. Mechanisms of alternative pre-messenger RNA splicing. Annu. Rev. Biochem. **72:**291–336.
3. **Buratti, E., and F. E. Baralle.** 2004. Influence of RNA structure on the pre-mRNA splicing process. Mol. Cell. Biol. **24:**10505–10514.
4. **Buratti, E., and F. E. Baralle.** 2005. Another step forward for SELEXive splicing. Trends Mol. Med. **11:**5–9.
5. **Cartegni, L., and A. R. Krainer.** 2002. Disruption of an SF2/ASF-dependent exonic splicing enhancer in *SMN2* causes spinal muscular atrophy in the absence of *SMN1*. Nat. Genet. **30:**377–384.
6. **Cartegni, L., and A. R. Krainer.** 2003. Correction of disease-associated exon skipping by synthetic exon-specific activators. Nat. Struct. Biol. **10:**120–125.
7. **Cartegni, L., J. Wang, Z. Zhu, M. Q. Zhang, and A. R. Krainer.** 2003. ESEfinder: a web resource to identify exonic splicing enhancers. Nucleic Acids Res. **31:**3568–3571.
8. **Chen, X., L. Guo, W. Lin, and P. Xu.** 2003. Expression of Tra2β isoforms is developmentally regulated in a tissue- and temporal-specific pattern. Cell Biol. Int. **27:**491–496.
9. **Clark, F., and T. A. Thanaraj.** 2002. Categorization and characterization of transcript-confirmed constitutively and alternatively spliced introns and exons from human. Hum. Mol. Genet. **11:**451–464.
10. **Crooke, S. T.** 2004. Antisense strategies. Curr. Mol. Med. **4:**465–487.
11. **Elbashir, S. M., J. Harborth, K. Weber, and T. Tuschl.** 2002. Analysis of gene function in somatic mammalian cells using small interfering RNAs. Methods **26:**199–213.
12. **Fairbrother, W. G., R. F. Yeh, P. A. Sharp, and C. B. Burge.** 2002. Predictive identification of exonic splicing enhancers in human genes. Science **297:** 1007–1013.
13. **Faustino, N. A., and T. A. Cooper.** 2003. Pre-mRNA splicing and human disease. Genes Dev. **17:**419–437.
14. **Forte, A., M. Cipollaro, A. Cascino, and U. Galderisi.** 2005. Small interfering RNAs and antisense oligonucleotides for treatment of neurological diseases. Curr. Drug Targets **6:**21–29.
15. **Garcia-Blanco, M. A., A. P. Baraniak, and E. L. Lasda.** 2004. Alternative splicing in disease and therapy. Nat. Biotechnol. **22:**535–546.
16. **Graveley, B. R.** 2000. Sorting out the complexity of SR protein functions. RNA **6:**1197–1211.
17. **Helmken, C., Y. Hofmann, F. Schoenen, G. Oprea, H. Raschke, S. Rudnik-Schoneborn, K. Zerres, and B. Wirth.** 2003. Evidence for a modifying pathway in SMA discordant families: reduced SMN level decreases the amount of its interacting partners and Htra2-β1. Hum. Genet. **114:**11–21.
18. **Hofmann, Y., C. L. Lorson, S. Stamm, E. J. Androphy, and B. Wirth.** 2000. Htra2-β1 stimulates an exonic splicing enhancer and can restore full-length SMN expression to survival motor neuron 2 (SMN2). Proc. Natl. Acad. Sci. USA **97:**9618–9623.
19. **Hofmann, Y., and B. Wirth.** 2002. hnRNP-G promotes exon 7 inclusion of survival motor neuron (SMN) via direct interaction with Htra2-β1. Hum. Mol. Genet. **11:**2037–2049.
20. **Hsieh-Li, H. M., J. G. Chang, Y. J. Jong, M. H. Wu, N. M. Wang, C. H. Tsai, and H. Li.** 2000. A mouse model for spinal muscular atrophy. Nat. Genet. **24:**66–70.
21. **Huang, Y., N. H. Shin, Y. Sun, and K. K. Wang.** 2001. Molecular cloning and characterization of a novel caspase-3 variant that attenuates apoptosis induced by proteasome inhibition. Biochem. Biophys. Res. Commun. **283:**762–769.
22. **Izquierdo, J. M., N. Majos, S. Bonnal, C. Martinez, R. Castelo, R. Guigo, D. Bilbao, and J. Valcárcel.** 2005. Regulation of Fas alternative splicing by antagonistic effects of TIA-1 and PTB on exon definition. Mol. Cell **19:**475–484.
23. **Jaeger, L. B., and W. A. Banks.** 2005. Transport of antisense across the blood-brain barrier. Methods Mol. Med. **106:**237–251.
24. **Kashima, T., and J. L. Manley.** 2003. A negative element in SMN2 exon 7 inhibits splicing in spinal muscular atrophy. Nat. Genet. **34:**460–463.
25. **Kole, R., M. Vacek, and T. Williams.** 2004. Modification of alternative splicing by antisense therapeutics. Oligonucleotides **14:**65–74.
26. **Kornblihtt, A. R.** 2005. Promoter usage and alternative splicing. Curr. Opin. Cell Biol. **17:**262–268.
27. **Lefebvre, S., L. Burglen, S. Reboullet, O. Clermont, P. Burlet, L. Viollet, B. Benichou, C. Cruaud, P. Millasseau, M. Zeviani, D. LePaslier, F. Frezal, D. Cohen, J. Weissenbach, A. Munnich, and J. Melki.** 1995. Identification and characterization of a spinal muscular atrophy-determining gene. Cell **80:**1–5.
28. **Lefebvre, S., P. Burlet, Q. Liu, S. Bertrandy, O. Clermont, A. Munnich, G. Dreyfuss, and J. Melki.** 1997. Correlation between severity and SMN protein level in spinal muscular atrophy. Nat. Genet. **3:**265–269.
29. **Lim, S. R., and K. J. Hertel.** 2001. Modulation of survival motor neuron pre-mRNA splicing by inhibition of alternative 3′ splice site pairing. J. Biol. Chem. **276:**45476–45483.
30. **Lorson, C. L., J. Strasswimmer, J. M. Yao, J. D. Baleja, E. Hahnen, B. Wirth, T. Le, A. H. Burghes, and E. J. Androphy.** 1998. SMN oligomerization defect correlates with spinal muscular atrophy severity. Nat. Genet. **19:**63–66.
31. **Lorson, C. L., E. Hahnen, E. J. Androphy, and B. Wirth.** 1999. A single nucleotide in the SMN gene regulates splicing and is responsible for spinal muscular atrophy. Proc. Natl. Acad. Sci. USA **96:**6307–6311.
32. **Lorson, C. L., and E. J. Androphy.** 2000. An exonic enhancer is required for inclusion of an essential exon in the SMA-determining gene SMN. Hum. Mol. Genet. **9:**259–265.
33. **Lu, Q. L., A. Rabinowitz, Y. C. Chen, T. Yokota, H. Yin, J. Alter, A. Jadoon, G. Bou-Gharios, and T. Partridge.** 2005. Systemic delivery of antisense oligoribonucleotide restores dystrophin expression in body-wide skeletal muscles. Proc. Natl. Acad. Sci. USA **102:**198–203.
34. **Mahotka, C., M. Wenzel, E. Springer, H. E. Gabbert, and C. D. Gerharz.** 1999. Survivin-ΔEx3 and survivin-2B: two novel splice variants of the apoptosis inhibitor survivin with different antiapoptotic properties. Cancer Res. **59:**6097–6102.
35. **Maniatis, T., and B. Tasic.** 2002. Alternative pre-mRNA splicing and proteome expansion in metazoans. Nature **418:**236–243.
36. **Mercado, P. A., Y. M. Ayala, M. Romano, E. Buratti, and F. E. Baralle.** 2005. Depletion of TDP 43 overrides the need for exonic and intronic splicing enhancers in the human apoA-II gene. Nucleic Acids Res. **33:**6000–6010.
37. **Mercatante, D. R., J. L. Mohler, and R. Kole.** 2002. Cellular response to an antisense-mediated shift of Bcl-x pre-mRNA splicing and antineoplastic agents. J. Biol. Chem. **277:**49374–49382.
38. **Miriami, E., H. Margalit, and R. Sperling.** 2003. Conserved sequence elements associated with exon skipping. Nucleic Acids Res. **31:**1974–1983.
39. **Miyajima, H., H. Miyaso, M. Okumura, J. Kurisu, and K. Imaizumi.** 2002. Identification of a cis-acting element for the regulation of SMN exon 7 splicing. J. Biol. Chem. **277:**23271–23277.
40. **Miyaso, H., M. Okumura, S. Kondo, S. Higashide, H. Miyajima, and K. Imaizumi.** 2003. An intronic splicing enhancer element in survival motor neuron (SMN) pre-mRNA. J. Biol. Chem. **278:**15825–15831.
41. **Monani, U. R., C. L. Lorson, D. W. Parsons, T. W. Prior, E. J. Androphy, A. H. Burghes, and J. D. McPherson.** 1999. A single nucleotide difference that alters splicing patterns distinguishes the SMA gene SMN1 from the copy gene SMN2. Hum. Mol. Genet. **8:**1177–1183.
42. **Monani, U. R., M. Sendtner, D. D. Coovert, D. W. Parsons, C. Andreassi, T. T. Le, S. Jablonka, B. Schrank, W. Rossol, T. W. Prior, G. E. Morris, and Burghes, A. H.** 2000. The human centromeric survival motor neuron gene (SMN2) rescues embryonic lethality in $Smn^{-/-}$ mice and results in a mouse with spinal muscular atrophy. Hum. Mol. Genet. **9:**333–339.
43. **Nilsen, T. W.** 2003. The spliceosome: the most complex macromolecular machine in the cell? Bioessays **25:**1147–1149.
44. **Nott, A., H. H. Le, and M. J. Moore.** 2004. Splicing enhances translation in mammalian cells: an additional function of the exon junction complex. Genes Dev. **18:**210–222.
45. **Pagani, F., E. Buratti, C. Stuani, and F. E. Baralle.** 2003. Missense, nonsense, and neutral mutations define juxtaposed regulatory elements of splicing in cystic fibrosis transmembrane regulator exon 9. J. Biol. Chem. **278:** 26580–26588.
46. **Pagani, F., C. Stuani, M. Tzetis, E. Kanavakis, A. Efthymiadou, S. Doudounakis, T. Casals, and F. E. Baralle.** 2003. New type of disease causing mutations: the example of the composite exonic regulatory elements of splicing in CFTR exon 12. Hum. Mol. Genet. **12:**1111–1120.
47. **Pagani, F., and F. E. Baralle.** 2004. Genomic variants in exons and introns: identifying the splicing spoilers. Nat. Rev. Genet. **5:**389–396.
48. **Park, V. M., K. A. Kenwright, D. B. Sturtevant, and E. K. Pivnick.** 1998. Alternative splicing of exons 29 and 30 in the neurofibromatosis type 1 gene. Hum. Genet. **103:**382–385.
49. **Sazani, P., and R. Kole.** 2003. Therapeutic potential of antisense oligonucleotides as modulators of alternative splicing. J. Clin. Investig. **112:**481–486.
50. **Singh, N. N., E. J. Androphy, and R. N. Singh.** 2004. An extended inhibitory context causes skipping of exon 7 of SMN2 in spinal muscular atrophy. Biochem. Biophys. Res. Commun. **315:**381–388.
51. **Singh, N. N., E. J. Androphy, and R. N. Singh.** 2004. In vivo selection reveals combinatorial controls that define a critical exon in the spinal muscular atrophy genes. RNA **10:**1291–1305.
52. **Singh, N. N., E. J. Androphy, and R. N. Singh.** 2004. The regulation and regulatory activities of alternative splicing of the SMN gene. Crit. Rev. Eukaryot. Gene Expr. **14:**271–285.
53. **Skordis, L. A., M. G. Dunckley, B. Yue, I. C. Eperon, and F. Muntoni.** 2003. Bifunctional antisense oligonucleotides provide a trans-acting splicing enhancer that stimulates SMN2 gene expression in patient fibroblasts. Proc. Natl. Acad. Sci. USA **100:**4114–4119.
54. **Sorek, R., and G. Ast.** 2003. Intronic sequences flanking alternatively spliced exons are conserved between human and mouse. Genome Res. **13:**1631–1637.
55. **Stoss, O., T. Novoyatleva, M. Gencheva, M. Olbrich, N. Benderska, and S. Stamm.** 2004. p59(fyn)-mediated phosphorylation regulates the activity of the tissue-specific splicing factor rSLM-1. Mol. Cell. Neurosci. **27:**8–21.
56. **Vinogradov, S. V., E. V. Batrakova, and A. V. Kabanov.** 2004. Nanogels for oligonucleotide delivery to the brain. Bioconjug. Chem. **5:**50–60.
57. **Wan, L., D. J. Battle, J. Yong, A. K. Gubitz, S. J. Kolb, J. Wang, and G.**

Dreyfuss. 2005. The survival of motor neurons protein determines the capacity for snRNP assembly: biochemical deficiency in spinal muscular atrophy. Mol. Cell. Biol. **25:**5543–5551.
58. **Wang, Z., M. E. Rolish, G. Yeo, V. Tung, M. Mawson, and C. B. Burge.** 2004. Systematic identification and analysis of exonic splicing silencers. Cell **119:** 831–845.
59. **Young, P. J., C. J. DiDonato, D. Hu, R. Kothary, E. J. Androphy, and C. L. Lorson.** 2002. SRp30c-dependent stimulation of survival motor neuron (SMN) exon 7 inclusion is facilitated by a direct interaction with hTra2β1. Hum. Mol. Genet. **11:**577–587.
60. **Yu, Q., J. Guo, and J. Zhou.** 2004. A minimal length between *tau* exon 10 and 11 is required for correct splicing of exon 10. J. Neurochem. **90:**164–172.
61. **Zhang, X. H., and L. A. Chasin.** 2004. Computational definition of sequence motifs governing constitutive exon splicing. Genes Dev. **18:**1241–1250.
62. **Zhang, X. H., C. S. Leslie, and L. A. Chasin.** 2005. Dichotomous splicing signals in exon flanks. Genome Res. **15:**768–779.